ANOMOLOUS TWO-PHASE FLOW BEHAVIOR IN FRACTURED SANDSTONE EXPLAINED USING X-RAY COMPUTED TOMOGRAPHY

Freddy E. Alvarado[1], Abraham S. Grader[2], Phillip M. Halleck[3]

[1] British Petroleum, Av. Francisco de Miranda. Edif. Centro Seguros Sud Americana, Piso 5. Caracas, Venezuela. [2] The Pennsylvania State University, 203 Hosler, University Park, PA 16802, USA. [3] The Pennsylvania State University, 152 Hosler, University Park, PA 16802, USA

ABSTRACT

Understanding flow behavior in fractured porous media is necessary for accurate simulation of multiphase transport in fractured rocks. Although ambient stress methods for obtaining fracture morphology exist, previous research lacks the ability to map fracture closure as a function of stress or the distribution of immiscible phases in the fracture. A twenty-five-millimeter cylindrical sandstone sample was artificially fractured in tension and placed under confining stress in an x-ray transparent vessel. The fracture morphology was defined under dry conditions using high-resolution x-ray computed tomography. Multi-phase fluid distributions in the fracture were mapped between limits of the mobile saturation range using controlled fractional flows. These distributions were correlated with flow-rate and pressure-drop measurements. We observed order-of-magnitude differences in effective permeabilities under conditions of nearly constant overall fracture saturations. These differences in permeability can be associated with re-arrangement of the physical distribution of the phases. Distributions associated with low permeability are unstable on a time frame of several hours - much longer than the time frame associated with snap-off phenomena. This instability may be responsible for similar field observations reported in the literature.

INTRODUCTION

Witherspoon *et al.* (1980), used a parallel plate approximation for studying fracture flow. They found an expression proportional to the cube root of fracture aperture, known as the cubic law, was suitable for a tight fracture under stress. However, more recent studies have questioned the validity of this cubic law given the complex geometry of fractures. The surface roughness and fracture aperture distributions play a key role in the conductivity of the fracture and its mechanical behavior during changes in confining pressure. Previous attempts to describe fracture apertures and fluid distribution have failed as a consequence of the heterogeneities of the porous media. High-resolution CT of samples during fluid flow can obtain the fracture morphology as well as the distribution of the phases within it, Alvarado *et al.* (2004).

EXPERIMENTAL METHODS AND PROCEDURES

We have undertaken a series of experiments on artificially fractured sandstone samples, measuring fracture morphology, relative permeabilities, and fluid distributions under low and high confining stresses. Basic measurements included flow-rates, pressure drops and temperatures. High-resolution x-ray CT was used to map fracture morphology and fluid distributions in three dimensions. As part if this series of experiments, we performed fractional flow tests on a sample subjected to a confining stress of 17 MPa. An additional CT data set obtained for the sample under dry conditions (at the same confining stress) was used to extract the fracture structure itself.

Rock sample, fracture preparation, and fluids

A Berea sandstone sample was used for the experiment. The average permeability (prior fracturing) was about 100 mD. A core with a diameter of 50 mm was machined to a precision cylinder and artificially fractured using a modified Brazilian test. Then the sample was over-cored to a diameter of 25 mm and cut to a length of 70 mm. The two immiscible fluids used for this experiment were water tagged with NaI (7% by weight) and kerosene. The immiscibility of the two fluids resembles the interaction of the fluids present in a reservoir. These two fluids also provide a clear contrast in x-ray attenuation, allowing the CT partitioning of the phases in the fracture.

Core holder, injection pumps, and x-ray CT unit

In order to minimize x-ray attenuation, a carbon-fiber composite high-pressure core holder was used. For injection of the two fluid phases, a precision computer-controlled pump system was used (2 subsystems, two cylinders per fluid phase). The pump system provides continuous, pulse-free fluid flow over its entire operating pressure range. The industrial CT unit is a third-generation scanner in which the source and detector are fixed and the scanned object rotates. Resolution was optimized by placing the core as close as possible to the micro-focus x-ray source. Ultimate resolution is controlled by the size of the source spot, so that a micro-focus tube produces a great advantage. High-resolution two-dimensional slices were reconstructed into 1024x1024 pixel elements. Several (41) slices were acquired per rotation, and the entire sample was scanned with the appropriate number of rotations to provide a complete three-dimensional virtual core.

Experimental procedure

The two halves of the core were displaced along its axis by 0.4 mm to increase fracture aperture and reduce asperity contacts. Then the sample was inserted into the core holder, and a confining stress of 3.5 MPa was applied to the dry sample. The core holder was mounted vertically in the scanner and connected to the fluid flow and monitoring systems. The sample was first scanned in the dry condition to provide the best conditions for extracting the virtual three-dimensional fracture. The sample was then vacuum-saturated with NaI solution and absolute permeability of the fractured sample was measured. At this point, several traverses of the oil/water factional flow curve were performed at a fixed overall flow rate, and full CT scans of the sample were acquired at residual water and residual oil conditions, and at several steady-state oil-water fractional flow conditions. Flow rates, pressure drops, and temperatures were continuously measured during the experiment. All flow tests reported in

this paper were done at a constant confining stress and at fixed overall injection rate. This procedure is only part of an experimental sequence that included variations of confining stress and fluid injection rates.

ANALYSIS

Fracture Aperture

Figure 1 shows a photograph (left) of the one-inch core before it was placed in the core holder and a sample x-ray CT slice that includes the fracture (center). The white rectangle highlighted on the center CT image was extracted and is shown on the right side of Figure 1. This rectangle with dimensions of 800x100 reduced the overall size of the data set by a factor of six, and simplified the computational procedures.

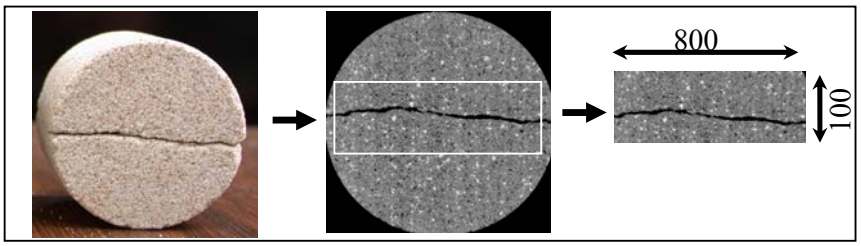

Figure 1: Original core before and after scanning and an extracted region that contains the fracture

The entire sample required about 2200 slices to create a virtual fracture. The voxel dimensions of the data were 0.036 x 0.026 x 0.031 mm in x-y-z directions, respectively. The fracture was defined using threshold methods and the entire virtual object was reduced to a binary representation in which the fracture had a value of one and the rest of the sample had a value of zero. The computed fracture volume was 83.2 cubic millimeters with 5.69 % of the area occupied by asperities at 3.5 MPa. Figure 2 shows a three-dimensional rendition of the fracture in which the black areas are asperities (areas of contact between the two parts of the sample).

Using the fracture aperture distribution, Zimmerman *et al.* (1991) suggested that the roughness of the fracture can be represented by the fractional standard deviation of the aperture distribution: *Roughness Factor* $= \sigma_m / a_m$, where σ_m represents the standard deviation and a_m the average aperture. A perfect parallel model has uniform fracture aperture and therefore a zero standard deviation, leading to a zero roughness factor. In the current case, the roughness factor for a confining stress of 3.5 MPa was 1.06. The roughness factor increased with confining pressure as the standard deviation increased and the aperture decreased.

The partitioned virtual fracture was used to provide the volume base for constraining the distribution of oil and water during two-phase flow tests. Mechanical registration was maintained throughout the tests so that mathematical operations involving images taken at different times can be performed.

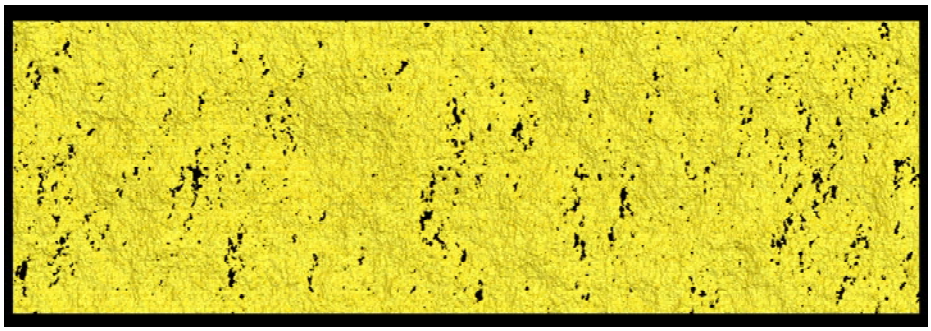

FIGURE 2. A top view of a three-dimensional rendition of the fracture at 3.5 MPa. Black regions are asperities.

Fluid flow experiments

After the sample was vacuum saturated NaI solution was injected to establish the single-phase permeability. Subsequently, oil viscosity was 0.953 cP and water viscosity was 1.006 cP. The pressure drop was measured at ports on the two faces of the core. The parallel plate approximation, Witherspoon *et al.* (1980), has been used to predict and interpret the pressure drop along fracture during single-phase flow. The cubic law equation is:

$Q = \Delta p b^3 W / 12 \mu L$, where μ is the dynamic viscosity of the fluid [$ML^{-1}T^{-1}$], L is length of the sample [L], W is the diameter of the sample [L], Q is the flow rate [L^3T^{-1}], Δp is the differential pressure [$ML^{-2}T^{-1}$], and *b* [L] is the equivalent hydraulic aperture of the fracture. This equation was used to predict the pressure drop along the fracture using the fracture average aperture obtained from the CT data (b=0.264 mm at 3.5 MPa confining pressure). The computed pressure drop for a flow rate of 12 cc/min was 0.43 kPa. The pressure drop measured experimentally was 15.9 kPa. The considerable difference between the estimated cubic law and the measured value (a factor of 37) is due the complex morphology of the fracture.

The relative permeabilities for the oil and water at S_{wirr} and S_{or} and at fractional flow of f_w= 0.66, are shown in Figure 3. All relative permeability data correspond to a confining pressure of 3.7 MPa. The green dashed lines represent the x-shaped curves for relative permeabilities for oil and water, typically used for fractured systems. The blue and red lines represent the experimental relative permeabilities, for water and oil, respectively. A significant deviation from the straight line is observed for the k_{ro} curve. Simple x-shaped curves over estimate the permeability of the non-wetting phase. The mobile range at this low confining pressure (3.7 MPa) is about 70%. Later on in the experimental procedure, the confining pressure was raised to 15 MPa and the residual oil saturation increased and the mobile saturation was reduced to 48%. The residual water saturation experienced little change.

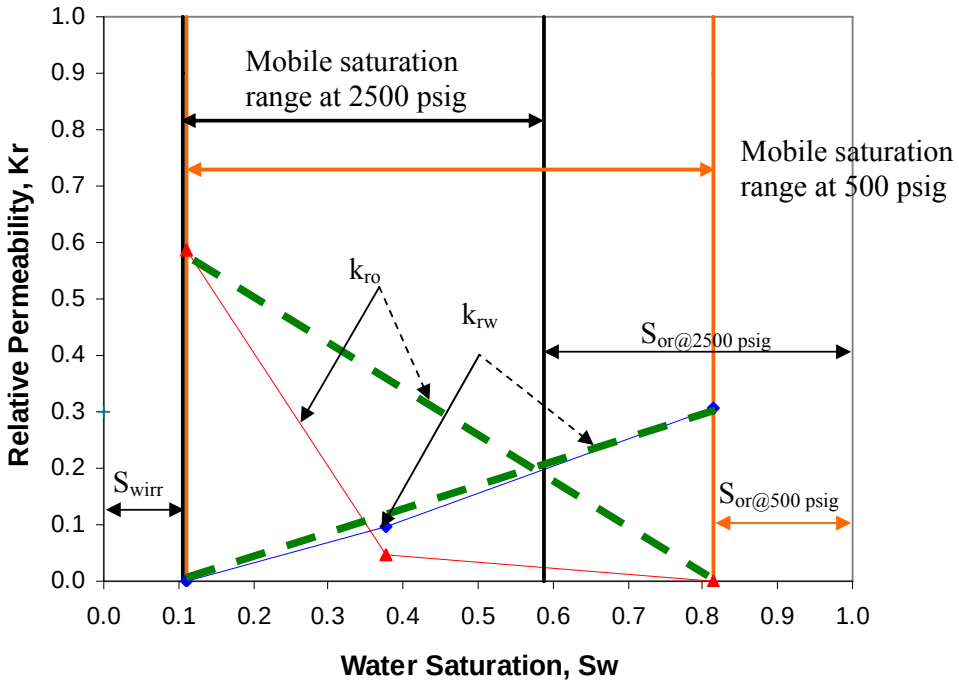

FIGURE 3. Relative permeability curves for a fractured system at 3.7 MPa.

After determining the relative permeabilities at residual water and at residual oil, different fractional flow injection sequences were performed in order to establish possible trends. The first sequence of fractional flow was done starting at fractional flow (water) equal 1.0 moving toward zero. Then the water fractional flow was gradually increased back to one. Each fractional flow traverse consisted of ten steady-state steps. Several full cycles of water fractional flow were performed. A total flow rate of 12 cc/min was used for this entire flow test.

We were unable to obtain repeatable drainage/imbibition loops. Pressure drops for each succeeding loop appeared to increase. We subsequently observed continuously increasing pressure drops at a constant fractional flow. This indicates a strong dependency of the relative conductivity of the fracture on drainage or imbibition processes and on changing saturation distribution with time. This behavior was observed repeatedly for upward flow. However, when the flow was reversed (downward flow) the pressure drop in the fracture dropped to its original value. When the upward flow direction was re-established a new build up of pressure drop was observed.

Scans of the injection and production ends of the sample showed no buildup of water or oil and that the end connectors were not responsible for the cyclic nature of the pressure drop along the fracture. The entire fracture was scanned at the start of the fractional flow cycle when the pressure drop was 6.9 kPa (low). Also, the sample was scanned at the maximum pressure drop of about 69 kPa, under the same fractional flow value and after several fractional flow cycles. Analysis of the average saturation in the core at the two pressure drop conditions yielded little change. The overall fluid saturations at the low pressure drop flowing conditions were 38.6 (S_{of}) and 61.4% (S_{wf}) for oil and water, respectively. The over

all fluid saturations at the high pressure drop flowing conditions were 37.8 (S_{of}) and 62.2% (S_{wf}) for oil and water, respectively. Thus, very similar overall saturation conditions were obtained while the pressure drops differed by an order of magnitude.

The x-ray CT data were used to compare the fluid distributions for these two extreme pressure drop conditions. Different non-connected or slightly-connected oil regions are shown in Figure 4 for low- and high-pressure-drop conditions. Figure 4b, high pressure drop, highlights the largest oil globule (red ellipse, yellow globule, between 20 and 30 mm above the injection end) with a volume of 9.3 mm^3, where most of the oil ganglia fall in the range between 0.01 and 0.09 mm^3. The same region in the low pressure drop condition does not show a large oil ganglion. This figure shows that although the overall saturation is about the same the distribution of the fluids is significantly different.

The saturation structure during the two-phase flow was not always stable. A sudden change in pressure drop was recorded at the end of an imbibition cycle during a steady injection. This significant loss in pressure drop could be produced by the displacement of oil globules (snap-off) in the fracture, and it was not possible to document it given that the CT time acquisition is much longer than time in which this event occurred. Reversing the flow direction in the fracture allows the fluids to rearrange and release the pressure buildup. This fracture plugging behavior can be directly related to problems with gas wells, where field data report possible water slugs plugging wells in hydraulically fractured gas reservoirs, Christiansen *et al.* (2005).

CONCLUSION

The distribution of the phases along the fracture modifies the relative conductivities of the fracture. The non wetting phase produces plugged regions that drastically reduce the multiphase conductivity of the fracture. This fracture plugging behavior can be directly related to problems with gas wells, where field data report possible water slugs plugging wells in hydraulically fractured gas reservoirs. The increase in confining stress caused significant increase in the residual oil saturation in the fracture. This increase in residual oil saturation (S_{or}) has a major effect on the change of relative permeabilities and on the mobile saturation range of a fracture. In the cases studied, relative permeabilities deviated significantly from the x-shaped curves typically used for fractures systems. In particular the conventional assumption grossly over predicts K_{ro}. Application of these observations should greatly improve accuracy of dual-permeability simulators.

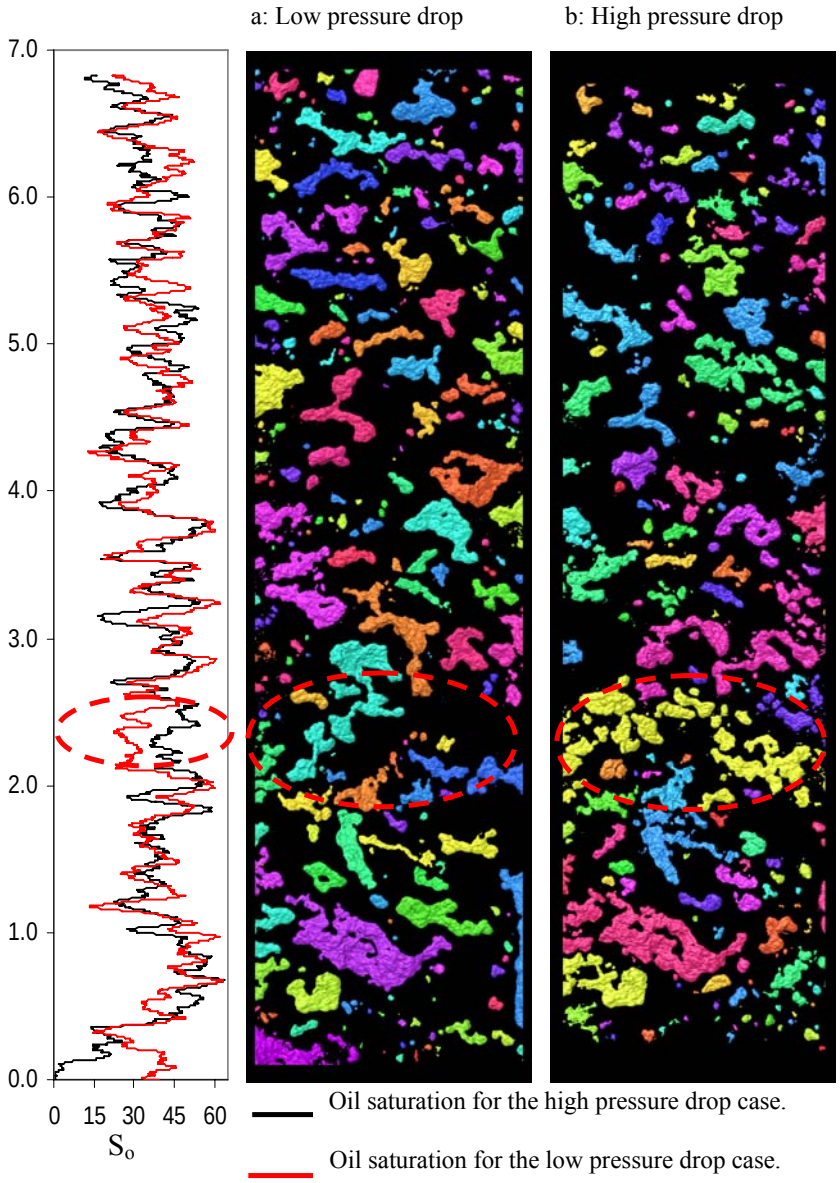

FIGURE 4. Oil distribution low pressure drop (a). Oil distribution high pressure drop (b).

REFERENCES

Alvarado, F. E., Grader, A. S., Karacan, O. and Halleck, P. M.: "Visualization of Three Phases in Porous Media Using Micro Computed Tomography," Petrophysics **45**, 2004.

Christiansen, R., Mayoral, C. and Pereira, C.: "Capillary End Effects and Gas Production From Low Permeability Formation," SCA, Canada, 2005.

Witherspoon, P. A., Wang, J. S. Y., Iwai, K. and Gale, J. E.: "Validity of cubic law for fluid flow in a deformable rock fracture," Water Resources Research **16**: 1016-1024, 1980.

Zimmerman, R. W., Kumar, S. and Bodvarsson, G. S.: "Lubrication theory analysis of the permeability of rough-walled fractures," International Journal of Rock Mechanics and Mining Science and Geomechanical Abstracts **28(B12)**: 325-331, 1991.